ELSEVIER

Fusion Engineering and Design 48 (2000) 281–298

Fusion Engineering and Design

www.elsevier.com/locate/fusengdes

Physics basis for a tokamak fusion power plant

S.C. Jardin [a,*], C.G. Bathke [b], D.A. Ehst [c], S.M. Kaye [a], C.E. Kessel Jr [a], B.J. Lee [d], T.K. Mau [e], J. Menard [a], R. Miller [e], F. Najmabadi [e]

[a] *Plasma Physics Laboratory, Princeton University, PO Box 451, Princeton, NJ 08543, USA*
[b] *Los Alamos National Laboratory, MS E526, Los Alamos, NM 87545, USA*
[c] *Argonne National Laboratory, 9700 S. Cass Avenue, Argonne, IL 60439, USA*
[d] *Korean Basix Science Institute, Taedok, South Korea*
[e] *University of California at San Diego, 9500 Gilman Drive, LaJolla, CA 92093-0417, USA*

Abstract

The five ARIES designs, which correspond to five different tokamak operating modes, are reviewed and compared. Physics figures of merit are introduced that quantify the major parameters of a tokamak design in a physics operating space. The five operating modes are compared to one another and to the existing tokamak data base in terms of these physics parameters. While the steady-state first stability design [ARIES-I] and the pulsed first stability design [PULSAR] are closest, no design has yet been completely prototyped in existing tokamaks. © 2000 Elsevier Science S.A. All rights reserved.

Keywords: Fusion power plant; Tokamak; Physics

1. Introduction

It is generally agreed that the tokamak magnetic confinement concept is presently the leading choice in the worldwide fusion program. However, there are at least five distinctly different tokamak operating modes that have been proposed for utilization in a deuterium/tritium fueled tokamak power plant. These five operating modes differ from one another in one or more of the following areas: (i) choice of stability regime (i.e. first regime, second regime, or mixed); (ii) choice of pulsed or steady state operation, and (iii) choice of conventional or low aspect ratio. While each of the five operating modes leads to a self-consistent design that is optimized within its unique set of design constraints, the five modes optimize to quite different plasma performance and engineering requirements.

The five tokamak operating modes that have been evaluated by the ARIES team are: (1) a steady state, first stability (FS) regime similar to ARIES-I [1]; (2) a pulsed (PU), first stability regime similar to PULSAR [2]; (3) a steady state, second stability (SS) regime similar to ARIES-II/IV [3]; (4) a steady state, reversed shear (RS) mode [4,5]; and (5) a steady state, low aspect ratio (LAR) configuration [6]. Each of the five operat-

* Corresponding author. Tel.: +1-609-2432635; fax: +1-609-2432662.
E-mail address: jardin@ppl.gov (S.C. Jardin).

PII: S0920-3796(00)00166-6

ing modes has a substantial theoretical basis involving the computation of self-consistent MHD equilibrium, ideal MHD stability, bootstrap current, and current-drive efficiency. However, not all of the five modes have been experimentally prototyped to the same degree.

We have identified a set of critical tokamak physics parameters called physics figures of merit (FOM). Comparing the FOM parameters for each of the five operating mode concepts with what has actually been obtained experimentally provides a way of assessing how credible the different designs are [7]. In the remainder of this paper, we summarize each of the five ARIES designs and their corresponding tokamak operating mode concepts, define and motivate the FOM parameters in each of the critical tokamak physics areas, and present figures comparing the physics parameters for the five concepts with the tokamak data base that has been assembled for ITER.

2. The ARIES designs

Each of the ARIES design concepts discussed in this section corresponds to a self-consistent power plant design optimized to its unique set of design choices. (Note, however, that the SS option has not been fully re-optimized after the β was lowered to conform to the disruption avoidance rule that the operating β be 10% below the stability limit. It is believed that, with an optimum equilibrium that minimizes the bootstrap current overdrive, the cost of electricity (COE) could be further reduced).

The COE values all came from the same systems code making the same assumptions regarding economics (e.g., material costs), engineering and materials (e.g., blanket thickness). [8]. The blanket and shield design used for four of the five power plant candidates is a refinement of the ARIES-II vanadium blanket and shield, while the LOW-A design utilizes a He-cooled ferritic steel design. While the absolute values for the COE reflect a high degree of uncertainty in material costs, we believe that the relative economic rankings of the five concepts are significant. However, it must be kept in mind, and will be discussed below, that the extrapolation in present day physics parameters needed to realize the five designs differs considerably.

2.1. First stability [ARIES-I]

The first stability tokamak power plant concept (FS) is a modification of the ARIES-I [1] design, but with the peak toroidal field at the coil lowered from the ARIES-1 value of 21 to 16 T. Additionally, the SiC blanket and shield have been replaced with the same vanadium blanket and shield as the other power plant candidates, for purposes of a common-base comparison. The normalized beta value is $\beta_N = 2.88$, (corresponding to $\beta/\varepsilon = 8.12$), which we calculate to be 10% below the beta limit that is self-consistent with the design pressure and current profiles without invoking conducting wall stabilization of the external kink mode. The values of $q_0 = 1.3$ and $q_* = 3.77$ were determined by a tradeoff between high β (and low q's) and high bootstrap fraction (and high q's). The design utilized relatively modest shaping parameters of $k_X = 1.8$ and $\delta_X = 0.7$ that allowed passive stabilization of the $n = 0$ axisymmetric instability of a double-null plasma with the stabilizer located behind the breeding blankets, and at the same time minimized the PF coil energy. A combination of ICRF fast wave and lower hybrid wave was used as the current drive system. The total current drive power required is high (237 MW) because of the relatively low bootstrap fraction of 0.57.

2.2. Second stability [ARIES-II]

The second stability tokamak power plant concept (SS) is an updated version of the ARIES-II [3] design, where a more accurate bootstrap current model [9] with full alpha pressure representation has been applied. As with the other options, the pressure is lowered to give a 10% margin against the MHD stability limit, and a refined vanadium blanket and shield design has been used. The design has a normalized beta value of $\beta_N = 5.28$ (assuming a wall stabilized external kink mode), but with high central and cylindrical safety-factor values of $q_0 = 2.0$ and $q_* = 4.6$ in

order to obtain the high values of $\varepsilon\beta$ needed for full second stability access. This design, which has not been re-optimized with respect to the COE, has a value of $\beta/\varepsilon = 12$, only about 50% higher than FS. But the boot strap-current fraction, f_{BC}, exceeds unity, with the equilibrium having a substantial bootstrap overdrive in the bulk plasma, and a plasma current of $I_p = 7.72$ MA, significantly enhancing the recirculating power over that of ARIES-II. The design uses a combination of ICRF fast-wave current drive to provide the seed current on axis and lower-hybrid current drive to offset the overdriven bootstrap, current in the bulk plasma region and to tailor the current profile near the edge.

2.3. Pulsed operation [PULSAR]

The pulsed tokamak power plant concept (PU) is a modification of the PULSAR [2] design, with a reduced normalized beta value of $\beta_N = 2.70$, ($\beta/\varepsilon = 8.12$), which we calculate to be 10% below the beta limit in the absence of a nearby conducting wall. The design also uses the common vanadium blanket and shield design that represents a refinement over the original PULSAR blanket and shield. The current profile is calculated self-consistently from the requirement that the plasma be in an ohmic stationary state with no external current drive, and that the bootstrap current and plasma resistivity be consistent with the pressure and the temperature profiles. The design utilized the same modest shaping of $k_X = 1.8$ and $\delta_X = 0.5$ as did the FS design. The recirculating power fraction is very low since the design uses only inductive current drive, which has very high efficiency. The fact that the tokamak is pulsed causes the design value of the peak field at the coil to be 18% lower than for steady state designs (FS), and the fact that there is no control over the current profile causes the β_N to be 6% lower.

2.4. Reversed shear [ARIES-RS]

The reverse shear tokamak power plant concept (RS) grew out of analysis performed for the TPX program [5]. Its combination of a current profile peaked off axis and a peaked pressure profile leads to a self-consistent design with a normalized beta value of $\beta_N = 4.84$ (assuming a wall stabilized external kink mode), and to a value of $\beta/\varepsilon = 20.0\%$, over twice as large as FS, but also to a value of the bootstrap-current fraction of $f_{BS} = 0.88$, leading to a very low recirculating power fraction. We expect this design to have favorable transport properties in light of the experimental results [10,11] showing greatly reduced transport in the reversed shear configuration. The shaping has a modest elongation and high triangularity with $k_X = 1.9$ and $\delta_X = 0.77$.

2.5. Low-aspect-ratio [ARIES-ST]

The low-aspect-ratio tokamak [6] (LAR) differs from the others in that the TF coils are made of normal-conducting copper rather than superconducting, and that there are no OH coils on the inboard side. Only minimal shielding is provided on the inboard side of the tokamak in order to maximize the volume that the TF conductor occupies. Detailed MHD stability calculations show that it is possible to find stable equilibria at low aspect ratios with high values of the normalized beta which simultaneously allows for high beta and high bootstrap fraction. The reference LAR design has an aspect ratio of $A = 1.6$, a normalized beta value of $\beta_N = 6.3$ (assuming a wall stabilized external kink mode), and a value of $\beta/\varepsilon = 56.5\%$, significantly larger than the other designs. The bootstrap current density profile is well aligned with the equilibrium current profile over most of the plasma cross section, so that the pressure-driven current (boot strap + diamagnetic) is calculated to be 99% of the plasma current, the seed current being located near the magnetic axis. As a result, the current-drive power requirement of 54.3 MW (low-frequency fast wave) is the lowest among the steady state candidates. (One caveat of this result could be that the CD power is extremely sensitive to variations in the plasma profiles.) Even with the low CD power, however, the large amount of power dissipated by the copper coils leads to a very large recirculating power fraction.

Table 1
Parameters for the five ARIES power plant designs

Parameter	FS	PU	RS	SS*	LAR
Plasma aspect ratio, $A = R\ a_p^{-1}$	4.0	4.0	4.0	4.0	1.60
Major radius, $R(m)$	7.96	8.68	5.52	6.40	3.20
Plasma minor radius, a_p (m)	1.99	2.17	1.38	1.60	2.00
Plasma elongation, κ_X	1.81	1.80	1.89	2.03	3.44
Plasma triangularity δ_X	0.71	0.50	0.77	0.67	0.60
Cylindrical safety factor, q_*	3.77	2.40	2.37	4.60	3.13
Central safety factor, q_0	1.3	0.7	2.8	2.0	3.0
Stability parameter, $\varepsilon\beta_p$	0.54	0.32	0.57	1.22	0.99*
Normalized beta, β_N (%)	2.88	2.70	4.84	5.28	6.30
ITER-89P scaling multiplier, H	1.71	2.38	2.33	2.47	2.74
Plasma current, I_p (MA)	12.6	15.0	11.3	7.72	31.2
Bootstrap-current fraction, f_{BS}	0.57	0.34	0.88	>1	0.99
CD powerto plasma, P_{CD} (MW)	236.6	0	80.7	199.1	54.3
On-axis toroidal field, B_T (T)	8.99	7.46	7.98	8.37	2.78
Peak field at TF coil, B_{TF} (T)	16.0	13.1	15.8	15.9	11.7
Recirculating power fraction, $(1/Q_E)$	0.29	0.06	0.17	0.33	0.51
Total COE (ml kWH^{-1})	99.7	130.2	75.6	92.6	117.6

* This design is not optimized to the lowest COE.
** Includes diamagnetic current.

2.6. Summary of operating parameters

Operating parameters, dimensions and COE as determined by the ARIES systems code for the five tokamak power plant concepts are summarized in Table 1. From this table, we see that with common engineering assumptions applied to the five designs, the projected COE differs considerably, with the RS design being the most attractive, followed by the SS, the FS, the LAR, and the PU design. However, as is shown in Section 4, the physics design parameters for the five designs are not all on the same experimental basis.

3. Physics figures of merit

The performance properties and hence the economics of a power plant will be strongly affected by the baseline tokamak physics parameters. These are significantly different for each of the five candidate designs. For the power plant to be both economically attractive and physically credible, several of these parameters must be at or near their allowable limits, but none may exceed them. In an attempt to quantify this and to aid in concept selection, five critical areas of tokamak physics have been identified. In each of these areas, we have further identified one or more critical parameters, or FOM, which are dimensionless (wherever possible) measures of how close to the theoretical limits a tokamak can be operated. Before the detailed engineering design can proceed, there must be sufficient experimental data in place to demonstrate that a tokamak can operate reliably with the design values of the FOMs in the five critical areas. Thus, by comparing the FOMs of the five candidate designs with the existing tokamak data-base we can determine the relative credibility of the five designs. In addition, identification of these critical parameters should help focus present research efforts in the direction of optimizing and improving these quantities in existing and planned experiments in order to lead the way to a more attractive concept. The five critical physics areas are (A) MHD stability, (B) current drive, (C) power exhaust, (D) plasma energy confinement, and (E) particle confinement/helium ash removal. The relevant FOMs are discussed in the following subsections.

3.1. MHD stability

There are advantages to operating a tokamak at high values of β/ε to achieve high fusion power density, p_f, and at high values of $\varepsilon\beta_p$ to achieve a high bootstrap current fraction, and consequently low recirculating power. Here β is the plasma beta defined as $2\mu_o\langle p\rangle/B_T^2$ and β_p is the poloidal beta given by $8\pi^2 a_p^2\langle p\rangle S/\mu_o I_p^2$, where $\langle p\rangle$ denotes the volume averaged pressure, B_T is the toroidal field in vacuum at the plasma major radius R, I_p is the total plasma current, S is the shape factor $(1+\kappa^2)/2$, ε is the inverse aspect ratio ($A^{-1}\equiv a_p/R$), a_p is the minor radius, and κ is the elongation. Another useful quantity that will be used in this subsection is the cylindrical safety factor, $q_* = 2\pi a_p^2 B_T S/\mu_o R I_p$.

It should be noted that β/ε, and not β, is a parameter of fundamental importance. It is well known that if the MHD equilibrium and stability equations are expanded in a self-consistent inverse-aspect-ratio ordering that allows pressure driven instabilities to be present, the so-called high-β ordering [12], then the tokamak β is of order ε and the β_p is of order ε^{-1}. Thus, to leading order in the expansion parameter ε, the equilibrium and stability properties of a high-β tokamak configuration depend only on β/ε and on $\varepsilon\beta_p$.

Furthermore, it follows that β/ε is the critical parameter if one assumes that the fusion power density p_f scales as $\beta^2 B_T^4$, and that the limiting value of B_T scales like $\varepsilon^{-1/2}$. This scaling for the maximum field strength at the plasma center comes from assuming that in a tokamak power plant, the maximum toroidal field will be limited by the requirement that the maximum field strength at the superconducting TF coil is below some critical value, B_{crit}. Assuming that the outermost part of the inside leg of the TF coil and the inside edge of the plasma are separated by shielding, etc. which occupies about 20% of the major radius, leads to a dependence of field strength on inverse aspect ratio which is very well approximated by $\varepsilon^{-1/2}$ for the range of aspect ratios: $2.5 \le A \le 5$.

It is cautioned in passing that profile effects that affect the fusion power density have been ignored here. The true fusion power output from a DT plasma would be better approximated by $\langle p^2\rangle$ than by $\langle p\rangle^2$ as has been done here. The latter quantity has been chosen for the simplifications it yields, and for its ease of measurement in existing experiments. However, care must be used in applying the results discussed here to tokamak equilibria with extreme ratios of $\langle p^2\rangle$ to $\langle p\rangle^2$.

Increasing $\varepsilon\beta_p$ in a given tokamak will normally increase its ratio of toroidal current driven by the bootstrap effect to the total current, $f_{BS} = I_{BS}/I_p$. However, the bootstrap fraction actually scales as $f_{BS} \propto C_{BS}\varepsilon\beta_p/\sqrt{\varepsilon}$ [13], where C_{BS} contains dependences on current, density, and temperature profiles. The factor $\sqrt{\varepsilon}$ reflects the decrease in bootstrap current as the aspect ratio is reduced.

There are limits on how much β/ε and $\varepsilon\beta_p$ can be increased, either separately or together. The beta limit, in the form $\beta \le C_T(I_p/B_T a_p)$, can be shown to be equivalent to the expression

$$(\varepsilon\beta_p)\left(\frac{\beta}{\varepsilon}\right) \le \left(\frac{C_T}{20}\right)^2 S \tag{1}$$

For a conventional first stability configuration (similar to PULSAR) with high current (low q_*) optimally shaped current and pressure distributions, and with sufficient triangularity in the cross-sectional shape, this equation must be obeyed with a Troyon coefficient of $C_T \simeq 3.5$. Plasma configurations with non-optimal profiles and shapes can be unstable at values of C_T considerably lower than 3.5. If a higher f_{BS} is desired for steady state operation, one can reduce the current or raise q_*, resulting in a lower β, as is the case with ARIES-I.

It may be possible to violate the Troyon limit if certain conditions are met which allow second stability as in ARIES-II, or at very large values of q_* [14] or at very low aspect ratios [15,16]. The conditions which allow second stability include either elevated central safety factor ($q_0 \ge 2$) [17], strong cross-sectional indentation [18], or reversed magnetic shear [5]. In addition to these requirements, stabilization of the external kink mode in a second stability plasma requires a close fitting conducting wall and sufficient plasma rotation [19] and/or an active feedback system [20].

Other constraints come from the fact that the equilibrium equation must be obeyed, which implies $\varepsilon\beta_p \leq 2$ and that the external kink mode can only be stable for $q_* \geq 2$. The expression relating these quantities for a plasma equilibrium is given by

$$\left(\frac{\beta}{\varepsilon}\right) = (\varepsilon\beta_p)\frac{S}{q_*^2} \tag{2}$$

It is natural to choose as the MHD figures of merit the parameter pair $(\beta/\varepsilon, \varepsilon\beta_p)$. Note that a systems analysis is required to choose where in this space the fusion power plant should operate. There will always be a tradeoff between high $\varepsilon\beta_p$ and high β/ε as described by Eq. (1), and the preferred design will most likely optimize at intermediate values of each. An explicit illustration of the tradeoff between high β and high β_p is given in [21], in which an economic analysis determines the values of these parameters that minimize the COE of a first stability equilibrium with an ARIES-I type of current drive performance.

3.2. Current drive

The theory for non-inductive current drive [22–24] demonstrates that the driven current density, j_{dc}, is proportional to the product of the local absorbed power density, p_{dc} and the local electron temperature, T_e, divided by the electron density,

$$j_{cd} = A_0 p_{cd}\frac{T_e}{n_e}\left(\frac{\tilde{j}}{\tilde{p}}\right) \tag{3}$$

Here $(\tilde{j}/\tilde{p})$ is a normalized local current drive efficiency defined in [22] and is a dimensionless function of the location in electron velocity space where momentum and energy are absorbed, and A_0 is a constant. In a steady state plasma where there is no applied loop voltage, the total non-inductively driven current, I_{CD}, is found by integrating the local driven current density, j_{cd}, over the plasma cross section:

$$I_{CD} = \gamma_{CD}(P_{CD}/\bar{n}_e R) \tag{4}$$

(Note that this may also be obtained by dimensional analysis [25]). Here P_{CD} is the total RF power delivered to the plasma, $\bar{n}_e$, is the line average density, and R is the major radius. With negligible bootstrap current (low β_p), the normalized current-drive (CD) efficiency, γ_{CD}, is a convenient measure of success in CD experiments. Reference to (Eq. (3)) shows roughly that $\gamma_{CD} \sim T_e(\tilde{j}/\tilde{p})$. For early lower hybrid CD experiments, the wave phase speed was far in excess of the electron thermal speed and $T_e(\tilde{j}/\tilde{p}) \propto N_\parallel^{-2}$, where $N_\parallel \sim \mathcal{O}(1)$ is the parallel index of refraction, which is the ratio of the speed of light to the wave phase speed along the magnetic field. At low plasma temperatures the relationship $\gamma_{CD} \propto N_\parallel^{-2}$ is due to the efficiency of generating current with relatively collisionless electrons, resonant with high-speed wave momentum input [22]. Hence γ_{CD} was independent of T_e, and was an appropriate parameter for comparing theory with the early experiments. Experiments on PLT, ASDEX, JT60, and other machines, clearly showed $\gamma_{CD} \propto N_\parallel^{-2}$ in this regime.

At higher T_e,(≤ 5 keV), currents are driven with momentum input close to the thermal speed of the electrons, and in this regime the CD efficiency becomes $\gamma_{CD} \simeq T_e(\tilde{j}/\tilde{p}) \simeq T_{e0}$. Detailed calculations of self-consistent steady state tokamaks [23] have refined the temperature dependence for a power plant ($T_{e0} \geq 15$ keV) to $\gamma_{CD} \propto T_{e0}^n$, where $0.6 \leq n \leq 0.8$, depending on details of the plasma and current density profiles.

At the high β_p typical of a tokamak power plant, the prospect for current drive improves significantly over the early experiments. The toroidal plasma current, I_p, now consists of two components, one generated by one or more non-inductive CD sources with power P_{CD} and the other due to the toroidal bootstrap effect, i.e. $I_p = I_{BS} + I_{CD}$. Thus an economically attractive power plant can be realized if both the CD efficiency and the bootstrap, current fraction are high. To account for these two factors, a more appropriate, bootstrap-enhanced CD figure of merit, γ_B, is proposed, which is the same as the conventional measure of current-drive efficiency (γ_{CD}) but with I_{CD} replaced by I_p, and is given by

$$\gamma_B = (\bar{n}_e/10^{20})I_p R/P_{CD} \tag{5}$$

where SI units are used. It is clear from (Eq. (5)) that γ_B can be made large if a large part of I_p is

due to the bootstrap effect, i.e. if f_{BS} is large. The expression γ_B can be viewed as a global integral of the CD efficiency over the plasma minor cross section, including the bootstrap contribution. Thus, to lowest order, γ_B depends on the plasma equilibrium and on the electron temperature, T_e; to next order, it depends on details such as current drive techniques, plasma Z_{eff}, and equilibrium T_e and n_e, profiles. It is noted that in cases where the bootstrap current fraction is small ($f_{BS} \ll 1$), the conventional current drive efficiency is given by $\gamma_{CD} = \gamma_B(1 - f_{BS})$.

3.3. Heat exhaust

The need to remove the charged-particle heat escaping the tokamak plasma is an issue of critical importance in designing a fusion power plant. The bulk plasma is continuously heated by several hundred megawatts of power, P_α, coming both from the 3.5 MeV α-particles produced by the DT reactions, and from the external auxiliary power, P_{CD}, being applied for current generation. In order to remove this power, the conventional approach is to simultaneously radiate the power through atomic processes and magnetically divert the escaping charged particles and remaining heat flux through the scrape-off layer (SOL) to the divertor solid target plates. The average heat flux striking the divertor plate is approximated by

$$q_{PLATE} = \frac{1}{2\pi\lambda_{div}} \frac{P_{PLATE}}{R} \tag{6}$$

where λ_{div}, is the expanded power scrape-off scale length measured along the divertor plate, R is the major radius, and P_{PLATE} is the net power reaching the divertor plate. As a point of reference, the engineering design goal for fusion power plants is to limit the peak heat flux at the plates to less than 5 MW m^{-2}. Denoting P_{tr}, as the particle heat flux that crosses the separatrix and f_{rad} as the fraction of the total plasma heating power, $P_\alpha + P_{CD}$, that is radiated, then

$$P_{tr} = (P_\alpha + P_{CD})[1 - f_{rad}] \tag{7}$$

If there is no radiation in the scrape-off layer and the divertor region, then $P_{plate} = P_{tr}$. In this case, f_{rad} values of about 0.8 to 0.9 are necessary for a tokamak power plant in order to satisfy the above engineering design goal. This value of f_{rad} can be achieved by introducing impurities in the plasma edge creating a radiative edge mantle. However, the presence of these impurities can increase the current-drive power substantially. Another way to reduce the peak heat flux is to introduce impurities into the divertor region and allow for friction forces to entrain the impurities in the divertor region without increasing the Z_{eff} of the core plasma dramatically.

The atomic physics processes of potential importance in the plasma and divertor chamber include bremsstralilung and impurity line radiation, and charge exchange. Since the excitation energies of these processes are fixed constants, the ratios between the reference plasma temperature and these values are determined by the absolute magnitude of the former. Lackner [26] has extended this observation to demonstrate that under the condition of constant (or known) plasma temperature, similarity laws are obeyed in the plasma edge with the result that the quantity P_{tr}/R is in fact equivalent to the dimensionless figure-of-merit that characterizes the regime of divertor operation. This figure of merit has also been independently derived [27] by using the scaling transformation properties of the system of two dimensional fluid plasma and neutral equations together with boundary conditions [28].

We therefore can use the quantities P_{tr}/R and f_{rad} as figures of merit for comparing the divertor heat removal requirements in a given power plant candidate to the existing experimental database. It is essential that reactor-level values of both of these parameters be obtained simultaneously in order to demonstrate feasibility. An important caveat is that this must be achieved without a significant buildup of the injected impurity in the core. This is characterized by the requirement that $Z_{EFF} < 2.6$ for low-Z impurities. Attainment of these parameters will likely involve a splitting of the radiating power between the plasma center, mantle, SOL, and divertor, and will also likely require density compression of the impurity species in the divertor region.

3.4. Energy confinement

Plasma energy confinement is one of the most important issues for a fusion power plant design, but is not yet well understood. It is measured by the global energy confinement time, τ_E, which is defined as the time for the transport of plasma energy across the confining magnetic field, from the core to the edge region. From a single particle orbit perspective, the value of τ_E depends intrinsically on the size of the toroidal plasma, and on the magnitude of the confining magnetic field. However, the actual level of energy confinement is governed by the detailed transport processes induced by drift wave turbulence and micro-instabilities due to various plasma gradients and the presence of magnetically trapped particles. As a result, the tokamak plasma can exhibit a variety of confinement modes.

There are two classes of plasma confinement regimes in tokamak discharges that involve auxiliary heating power. The first class includes L-mode discharges where the energy confinement is low and where no attempt is made to improve the confinement by external means. The second class includes regimes with enhanced confinement (quiet H-mode, ELMy H-mode, Supershot, PEP H-mode, high-β_p H-mode, VH-mode, enhanced reversed shear mode, etc.). In general, better energy confinement leads to a more compact, and potentially more economical fusion power core, although the actual limits may be due to MHD stability limits or to engineering limits on the allowable heat flux or on the neutron wall loading.

Among the various energy confinement regimes, L-mode discharges have been studied most extensively. As part of the ITER Conceptual Design Activities, an empirical τ_E scaling [29] was obtained from a large number of tokamak L-mode discharges with different heating methods (NBI and RF) and different exhaust configurations (divertor and limiter), using an ordinary least squares regression technique. This confinement time scaling is given by

$$\tau_{ITER89-P} = 0.048 I_p^{0.85} R^{1.2} a_p^{0.3} \kappa^{0.5} \bar{n}_{20}^{0.1} B^{0.2} A_i^{0.5} P^{-0.5} \quad (8)$$

where SI units are used, $\bar{n}_{20}$, A_i and P are the line-averaged electron density (10^{20} m^{-3}), ion mass number, and total heating power (MW), respectively, and I_p is in MA.

On the other hand, except for the quiet and ELMy H-modes, confinement scalings for the enhanced confinement regimes of operation have yet to be established. This is partly because of an insufficient database and partly because many of these discharges rely on detailed control of the plasma profiles that may require a new methodology to parameterize. The reference ITER plasma operational regimes [30] will be based on the ELMy H-mode confinement regime in order to ensure ignition with a modest heating power requirement and moderate ash buildup in the plasma. However, unlike ITER which has a relatively conservative near-term goal, selection of the power plant operation scenario will require the consideration of a much broader range of enhanced confinement modes in order to maximize its economic potential.

An important consideration for ignition devices (such as ITER) and fusion power plants is the plasma pressure $\langle p \rangle = \langle nT \rangle$ at which these enhanced confinement modes are achieved. For ion temperatures in the range of 5–25 keV, typical of a DT burning power plant, the fusion power is proportional to $\langle nT \rangle$. Using simple power balance, the ratio of fusion power to the rate at which energy is conducted away is proportional to $\langle nT \rangle \tau_E$, which more appropriately characterizes the confinement capacity for a fusion plasma than τ_E alone. As an example, the ITER-CDA device will require a confinement capacity of $T_{i0} n_{DT0} \tau_E \sim 4\text{–}8 \times 10^{21}$ keV s^{-1} m^{-3} for fusion $Q \sim 5 - \infty$. Using $\langle nT \rangle \sim \beta B_T^2$ and $\chi_E \sim a_p^2/\tau_E$, where χ_E is a volume averaged heat diffusivity, one can obtain:

$$\beta/\chi_E \sim \beta \tau_E / a_p^2 \sim \langle nT \rangle \tau_E / (a_p B_T)^2 \quad (9)$$

Note that in Eq. (9), the quantity $\beta \tau_E / a_p^2$ provides a normalized measure of the confinement capacity, by factoring out the dominant dependences of the device size and magnetic field. This parameter is also proportional to β/χ_E, which was previously proposed as a reactor figure of merit [31].

Another commonly used figure of merit for confinement capacity can be derived from the quantity $\langle nT\rangle\tau_E$, irrespective of machine size and easily measurable in present experiments. By invoking a 'generic' L/H-mode scaling [32] of $\tau_E \propto HIpR^{3/2}\kappa^{1/2}P^{-1/2}$, and noting that $P \propto (\langle nT\rangle/\tau_E)Ra_p^2\kappa$, one can derive the relation $\langle nT\rangle\tau_E \propto (HI_p/\varepsilon)^2$, where H is the mode confinement enhancement factor. Neglecting shape factors (δ, κ) and substituting $q_* \propto \varepsilon a_p B_T/I_p$ into the above expression yields the relationship

$$\langle nT\rangle\tau_E/(a_pB_T)^2 \propto (H/q_*)^2 \tag{10}$$

where H/q_*. is the desired figure of merit. However, the derivation of this figure of merit depends on the 'generic' L/H-mode scaling. Recently, the ITER H-mode Database Working Group derived global confinement scalings from various subsets of the H-mode confinement database and found that the parameter exponents can differ substantially from those of the ITER-89P L-mode scaling. For example, for ELMy H-modes, the thermal energy confinement scaling is found to be [33]:

$$\tau_{H-mode} = 0.045 I_p^{1.06} R^{1.79} \kappa^{0.66} \bar{n}_{20}^{0.17} B_T^{0.32} A_i^{0.41} P^{-0.67} \varepsilon^{-0.11} \tag{11}$$

where P is now the total heating power corrected for beam shine-through, orbit loss and charge exchange losses. Comparing Eq. (8) and Eq. (11) illustrates that there is substantial variation from the 'generic' L/H-mode scaling and that the use of H/q_*. as a figure of merit is not universally applicable.

The cost of operating a fusion power plant is strongly dependent on the achievable fusion power density. Therefore, we propose plotting the confinement figure of merit β_{τ_E}/a_p^2 as a function of β/ε.[1] Simultaneous attainment of high confinement capacity and high fusion power density will then place the desirable region of operation in the upper right-hand quadrant of such a graph. This also serves as a guide to present and near-nerm experiments aimed at simulating attractive reactor confinement performance.

3.5. Helium ash removal

One of the major concerns for a fusion power plant is the effective removal of the helium ash produced by the fusion reactions [35–37]. It becomes increasingly difficult to maintain an ignited plasma the greater the helium concentration, due to dilution of the fuel ions and the enhanced radiation losses. It is well known that with helium present the energy confinement time must increase to compensate for the above effects.

From steady state helium particle balance in the core plasma, the ratio of helium to the fuel ion density is given by

$$\frac{n_{He}}{n_i} = \frac{\tau_{He}}{(1-R_{He})}\frac{n_i\langle\sigma_v\rangle}{4} \tag{12}$$

where n_i is the DT fuel ion density, n_{He}, is the helium density, $\langle\sigma_v\rangle$ is the fusion reaction rate, R_{He}, is the helium recycling coefficient, and τ_{He}, is the helium particle confinement time in the core plasma. Here all other impurities have been ignored.

From Eq. (12), the physical parameters that affect the core helium are τ_{He}, and R_{He}, which must both be made as small as possible. The ratio of the core plasma helium confinement time to $(1-R_{He})$ is referred to as the effective confinement time τ_{He}^*, This time constant has physical significance in that it reflects the mean residence time of a helium particle before finally being pumped out of the plasma chamber. Here the total plasma density is defined by $n_o = n_e + n_i + n_{He}$, and impurities are ignored until later. In addition, quasi-neutrality requires that $n_e = n_i + 2n_{He}$, and we assume a 50–50 mixture of deuterium and tritium for the present discussion. Profile effects are not included in this discussion.

The general scheme for removing the helium ash is to use a pumped divertor, where some fraction of the helium leaving the plasma core is pumped out of the chamber. The amount of helium that must be pumped with the divertor is given by

[1] This combination was first proposed by R. Goldston, PPPl (1994).

$$\Gamma_{\mathrm{He}} = \left(\frac{V_c n_{\mathrm{He}}}{\tau_{\mathrm{He}}}\right)(1 - R_{\mathrm{He}}) \tag{13}$$

where V_c, is the core plasma volume, and the first term in parentheses is the helium flow from the core plasma into the SOL and divertor. The second term is the fraction of the helium that is actually pumped out of the chamber. In steady state, the product of these two terms is equal to the helium production rate from fusion reactions in the core plasma.

The divertor pumping requirement is given by

$$n^p_{\mathrm{He}} S^{\mathrm{eff}}_{\mathrm{He}} + n^p_i S^{\mathrm{eff}}_i = \Gamma_{\mathrm{He}} + \Gamma_i \tag{14}$$

where S^{eff} is the eflective pumping speed ($\mathrm{m}^3\ \mathrm{s}^{-1}$), n^p is the neutral particle density at the pump aperture, and Γ_i is the amount of fuel ions that are pumped and is defined the same way as Eq. (13). Note that the divertor pumps both helium and fuel particles simultaneously, the amount of each being determined by their densities at the pump aperture. Directly related to this particle removal is particle fueling, in order to maintain a fixed fuel ion density in the plasma core,

$$\Gamma_{\mathrm{fuel}} = 2\Gamma_{\mathrm{He}} + \Gamma_i \tag{15}$$

Recycling large amounts of DT fuel compounds the requirements on the fueling system. In addition, if the ratio of the helium to the fuel particle densities at the pump aperture could be made larger than the ratio of helium to fuel ion densities in the core plasma, then helium removal would be more efficient.

To examine the impact of helium ash accumulation in a fusion power plant, one can use a simple power balance for the core plasma in steady state, by neglecting radiation and current drive power, ignoring any impurities other than helium, and by considering all plasma species to have the same temperature and energy confinement time. At fixed β, the ratio of energy confinement times with and without the presence of helium can be written as

$$\frac{\tau_{\mathrm{E}}^{\mathrm{wHe}}}{\tau_{\mathrm{E}}^{\mathrm{w/oHe}}} = \left(1 + \frac{3}{2}\frac{n_{\mathrm{He}}}{n_i}\right)^2 \tag{16}$$

Clearly the presence of helium in the core plasma requires an increased energy confinement time to maintain power balance.

Since many transport theories relate the particle confinement time to the energy confinement time, the ratio of $\tau^*_{\mathrm{He}}/\tau_{\mathrm{E}}$ is often used to measure the eflectiveness of core ash removal. From the simple power balance above and helium particle balance, one can derive

$$\frac{\tau^*_{\mathrm{He}}}{\tau_{\mathrm{E}}} = \frac{\dfrac{n_{\mathrm{He}}}{n_i}}{1 + \dfrac{3}{2}\dfrac{n_{\mathrm{He}}}{n_i}}\left(\frac{E_\alpha}{3kT}\right) \tag{17}$$

where E_α is the alpha birth energy (3.5 MeV). Eq. (17) shows that as τ^*_{He} increases, the helium fraction in the plasma core increases. However, as pointed out earlier, τ_{E} must then increase in order to maintain the operating point. This ratio is therefore the condition required on τ^*_{He} in order to achieve power balance in a DT fusion plasma with a given helium to fuel ion density ratio. The introduction of impurities and radiation leads to an even lower value of $\tau^*_{\mathrm{He}}/\tau_{\mathrm{E}}$ to maintain a fixed ratio of helium to fuel ions in the plasma.

The difficulty with constructing a figure of merit for helium ash removal lies with the fact that the negative impact of helium in the core plasma is not properly represented without an ignited plasma. The fusion power plant requirement for $\tau^*_{\mathrm{He}}/\tau_{\mathrm{E}}$ is determined by two constraints, helium particle balance and ignited plasma power balance. For a given amount of helium in the plasma there is a corresponding particle confinement time and energy confinement time. In present day experiments, the plasma energy confinement time is unaffected by the presence of the helium. Therefore care must be taken when drawing a direct correlation between the $\tau^*_{\mathrm{He}}/\tau_{\mathrm{E}}$ from an experiment to a power plant. The question arises whether the original energy confinement time in the experiment, properly scaled to the power plant parameters, would be sufficient to maintain ignition with the given helium fraction in the plasma.

With this difficulty in mind, it is recommended that that ratio $\tau^*_{\mathrm{He}}/\tau_{\mathrm{E}}$ be presented simultaneously with the value of $\beta\tau_{\mathrm{E}}/a_p^2$ which measures the energy confinement performance of the plasma. Knowing the range of $\beta\tau_{\mathrm{E}}/a_p^2$ values required for ignited plasma power balance would help to indicate how

well experiments are actually simulating the power plant situation.

The problem caused by non-helium impurities is the displacement of fuel ions by the impurity ions and their associated electrons. A reasonable measure for this is simply Z_{eff}, and this should be minimized as much as possible.

4. Relation to tokamak data base

The physics FOM parameters for the five designs are summarized in Table 2. We see there is a wide range of variation in the physics parameters between the different designs. In this section, we compare each of the designs to the data base in each of the critical physics areas.

4.1. MHD stability — comparison to data base

Fig. 1 plots the MHD stability FOM parameters from five tokamaks for long-pulse, ELMy H-mode discharges with high β and high bootstrap fraction, together with the design values for the five power plant options. Both the FS and PU concepts are seen to lie within the extremes of the values of the database. The RS parameters are close to what has been achieved in PBX-M, but both the LAR and SS operating points are far from the existing data. It is undoubtedly of significance that three designs that utilize a conducting wall to stabilize the external kink mode are the three that are furthest from the data base of what has been achieved in existing tokamaks. The beta limits in these designs would drop significantly if the conducting wall was not present in the analysis, and would bring them much closer to the existing data [15,38].

Several additional caveats must be kept in mind in the interpretation of this data. One is that the PBX-M data are based on highly indented plasmas ($i \simeq 0.25$), which do not extrapolate well to power plant regimes. The second is that the nature of MHD changes at very high plasma parameters, transitioning from a resistive regime where finite Larmor radius (FLR) effects affect stability to a collisionless regime where FLR effects are negligible. This fact makes the lower field results in smaller, present day experiments not completely relevant for prototyping the MHD regimes in a burning plasma. Another caveat is that the MHD time scales needed for plasma profiles to fully relax and for weakly unstable dissipative MHD instabilities to grow can be very long by today's standards, so that few if any of the discharges displayed in Fig. 1 are truly in steady state.

4.2. Current drive — comparison to data base

In Fig. 2 the most recent experimental data on ICRF fast wave current drive (FWCD) are plotted as γ_{CD} versus T_{e0}. Most of these data points come from DIII-D [39], where the plasma was pre-heated either by electron cyclotron waves or by neutral beam injection, and where a four-strap directional antenna is used. Preliminary FWCD data taken at Tore-Supra [40] and TFTR [41] are

Table 2
Physics figure merit parameters for the five ARIES power plant designs

Parameter	FS	PU	RS	SS*	LAR
Stability parameter, $\varepsilon\beta_{\text{p}}$	0.54	0.32	0.57	1.22	0.99
Beta parameter, β/ε (%)	8.12	10.00	20.0	12.17	56.5
Confinement ratio, $\tau^*_{\text{He}}/\tau_{\text{E}}$	10.0	10.0	10.0	10.0	10.0
Ignition parameter, $\beta\tau_{\text{E}}/\alpha_p^2$(% s m^{-2})	0.78	2.18	3.63	1.35	20
Normalized confinement multiplier, H q*	0.45	0.99	0.99	0.54	0.86
CD efficiency, γ_{B} (1020 A W^{-1} m^{-2})	0.56	NA	1.63	0.49	5.5
Normalized heat flux, Ptr/R MW m^{-1})	71.2	29.5	76.7	89.0	163
Effective charge Z_{eff}	1.65	1.75	1.69	1.64	1.93
Radiation fraction f_{rad}	0.15	0.30	0.17	0.13	0.40

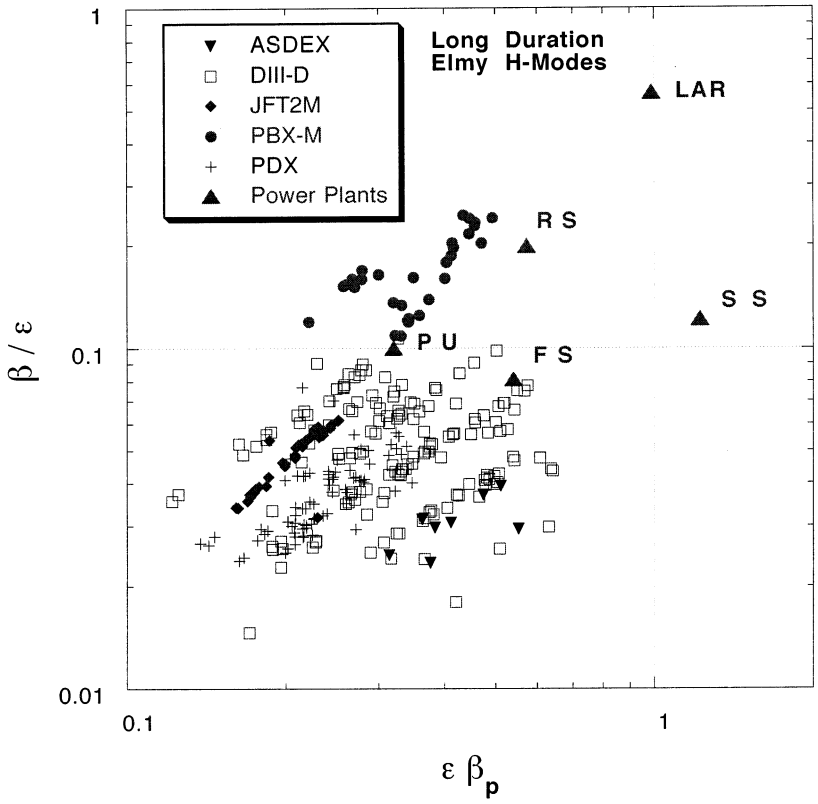

Fig. 1. MHD figures of merit for longer-pulse ELMy discharges in several existing devices and the five fusion power plant options.

displayed alongside the DIII-D data, and were obtained with two-strap 90° phased antennas in pre-heated plasmas. Also shown in this figure is the record value of $\gamma_{CD} = 0.45$ achieved to date on JET [42], when a synergistic combination of LH and ICRF power was used. For reference and comparison, the highest γ_B value of 0.34, achieved on JT-60 using LH power alone [43], is also displayed. On the same graph, the design values of γ_B (using a combination of RF techniques) for the FS, SS, RS and LAR power plant options are plotted, albeit at much higher values of T_{e0} than in present experiments. It is clear that considerable advances in the current drive database with fast wave power are required in order to reach the power plant regime. However, as the target plasma temperature improves with higher input power, and as the bootstrap fraction is raised in future devices, the value of the measured γ_B is expected to increase accordingly.

4.3. Heat exhaust — comparison to data base

Fig. 3 gives data points for heat removal in several tokamak experiments, where f_{rad} is plotted versus P_{tr}/R. In cases where there is no impurity injection [44], f_{rad} in the range of 0.4–0.6 is obtained by intrinsic carbon radiation in detached plasmas, e.g. on TEXTOR, C-Mod, ASDEX-U, JET, JT-60U and DIII-D. For discharges with neon puffing, such as in TEXTOR, ASDEX-U, and DIII-D, a total radiation fraction in the range of 0.9 is obtained. In the case of TEXTOR [45], where a pumped limiter was used, a radiating mantle was set up with a resultant $f_{rad} = 0.95$. Completely detached ELM-free H-mode experiments on ASDEX-U [46] show that f_{rad} can reach as high as 0.9 through a combination of D and Ne puffing, whereas f_{rad} drops to 0.55 without Ne puffing. In DIII-D [47], Ne puffing resulted in the simultaneous creation of a radiative mantle and a

strong radiation zone near the divertor plates, with each region radiating approximately equal power.

The range of design values of f_{rad} and P_{tr}/R for the five plant options are also plotted in Fig. 3. It is clear from this figure that the experimental database has already reached the desired value of f_{rad} for power plants, either by the action of a radiative mantle, or a combination of both SOL and core radiation. However, these data points have been achieved at levels of P_{tr}/R, that are still some distance away from those in power plants. If the peak solid target heat flux is to be limited to values less than 5 MW m^{-2}, a combination of enhanced radiation in the core, in the SOL, and in the divertor is required. The feasibility of obtaining this has not yet been demonstrated, but it may be possible using techniques such as impurity density compression in the divertor region.

4.4. Energy confinement — comparison to data base

In Fig. 4 the confinement FOMs are plotted for long pulse ELMy H-mode discharges on a number of devices together with the reference values for the five power plants designs. Note that the very favorable results for PBX-M are due to the highly indented plasma ($i \sim 0.25$) in those discharges. As indicated, the confinement performance of the FS option is well within those achieved on present machines, while the LAR power plant is farthest away from the existing database.

It must be pointed out that experimental databases on the RS and LAR concepts are not as developed as for the other tokamak concepts. For the reversed shear mode of operation, significant advances in plasma performance were reported

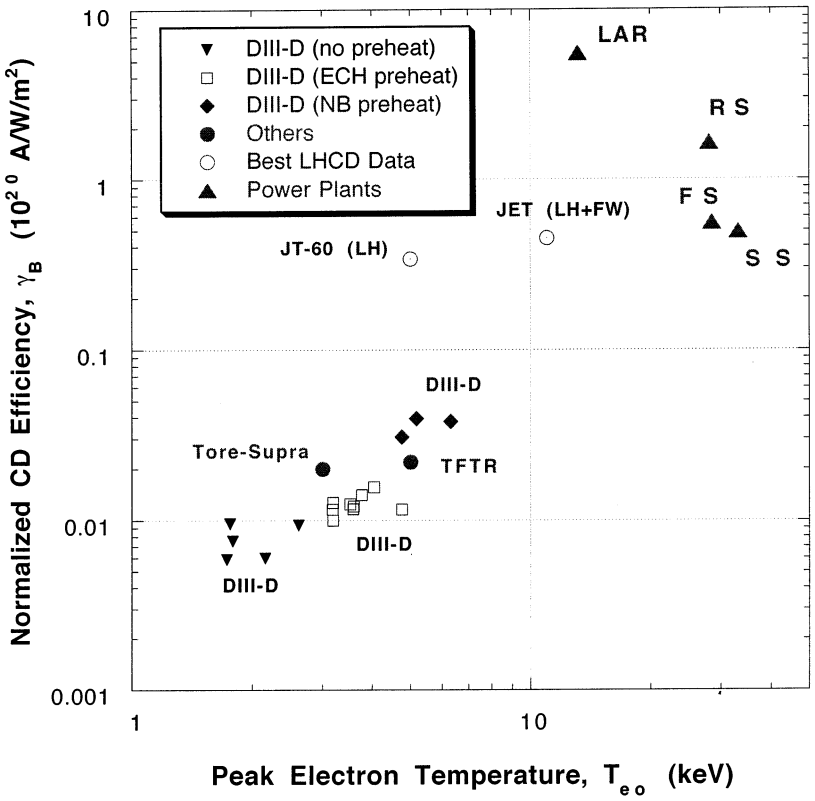

Fig. 2. Fast wave current-drive experimental database on DIII-D [39]; Tore Supra [40], and TFTR [41]; best data point for LHCD on JT-60 [43] and for LH and FW syneergy on JET [42]; and reference γ_B values for plant options.

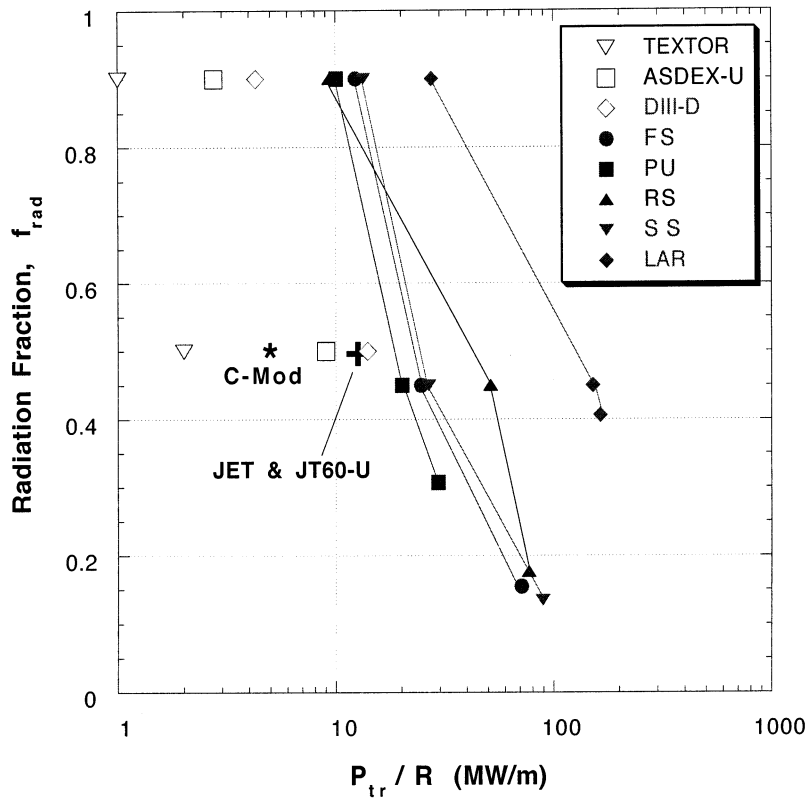

Fig. 3. Plot of heat exhaust figuresof merit, Frad versus Ptr/R, for a number of present experiments (TEXTOR, C-Mod, JET, JT60-U, ASDEX-U, and DIII-D), and design values for the five fusion power plants options (FS, PU, RS, SS, and LAR). The dotted and Chain-dotted lines represent the trend of PU options (FS, PU, RS, SAS and LAR). The dotted and chain-dotted lines represent the trend of PU option and LAR, respectively, due to the variation of frad. Options FS, RS, and SS follow the chained line. Note that frad of PU fusion power plant is relatively high compared to the other concepts because no CD power is required.

recently on TFTR [10] and on DIII-D [11]. Both experiments reported significant enhancements in energy confinement for both electrons and ions inside the RS region, leading to a highly peaked pressure profile near the axis. Of special interest are the DIII-D results which indicate transitions from the L-mode to the ELMY or ELM-free H-mode for these discharges with central reversed shear. This leaves open the possibility that the H-mode data presented in Fig. 4 may indeed be relevant to the RS mode. As for the LAR concept, the most advanced results have been from the START spherical tokamak [34], where the measured τ_E is typically twice the neo-Alcator value when ohmic heating alone is used. Data from double-null-divertor discharges on this machine appear to indicate transition to an improved confinement regime at high currents and densities. However, data on auxiliary heated discharges have not yet been incorporated into this assessment.

4.5. Helium ash removal — comparison to data base

The range of measured values for the helium-removal figure of merit on DIII-D [48–51] are shown in Fig. 5, as a function of $\beta\tau_E/a_p^2$. Also shown are the contours for ignited power balance, where a power plant can operate, at various volume-average temperatures. These results correspond to a reversed shear configuration with $A = 4.0$, $R = 5.6$ m, and $B_T = 7$ T. They include profile effects, and indicate that one needs to achieve low τ^*_{He}/τ_E

and high $\beta\tau_E/a_p^2$ simultaneously for fusion power-plant operation. Also displayed in Fig. 5 are the five power-plant candidates, for which $\tau^*_{He}/\tau_E = 10$ has been assumed, resulting in required $\beta\tau_E/a_p^2$ values ranging from 0.0078 for FS to 0.11 for LAR.

5. Summary and conclusions

To facilitate the assessment of the physics basis for a tokamak fusion power plant, we have introduced the concept of plasma performance parameters, or physics figures of merit (FOM). These have been identified in five critical physics areas: MHD stability, current drive, heat exhaust, energy confinement and helium ash removal. The FOMs have been applied to compare the physics assumptions made in five recent power plant designs for the ARIES team, namely ARIES-I, ARIES-II/IV, PULSAR, a reverse shear design, and the low-aspectratio configuration. We have labeled these FS, SS, PU, RS and LAR, respectively.

The FOMs can assist power-plant designers in evaluating the physics basis of their designs, and can assist the physics community by identifying what combinations of parameters are critical for an attractive tokamak power-plant. Hopefully, this will motivate experimental demonstrations of increased values of these parameters, and will also serve as a stimulus for new ideas on how to improve them. An attempt has been made to select the FOMs based on fundamental performance quantities that are readily measurable in experiments and that are independent of plasma size and machine-dependent parameters. The identified figures of merit are given as follows:

- MHD stability:
  - Power density parameter: β/ε
  - Stability parameter: $\varepsilon\beta p$

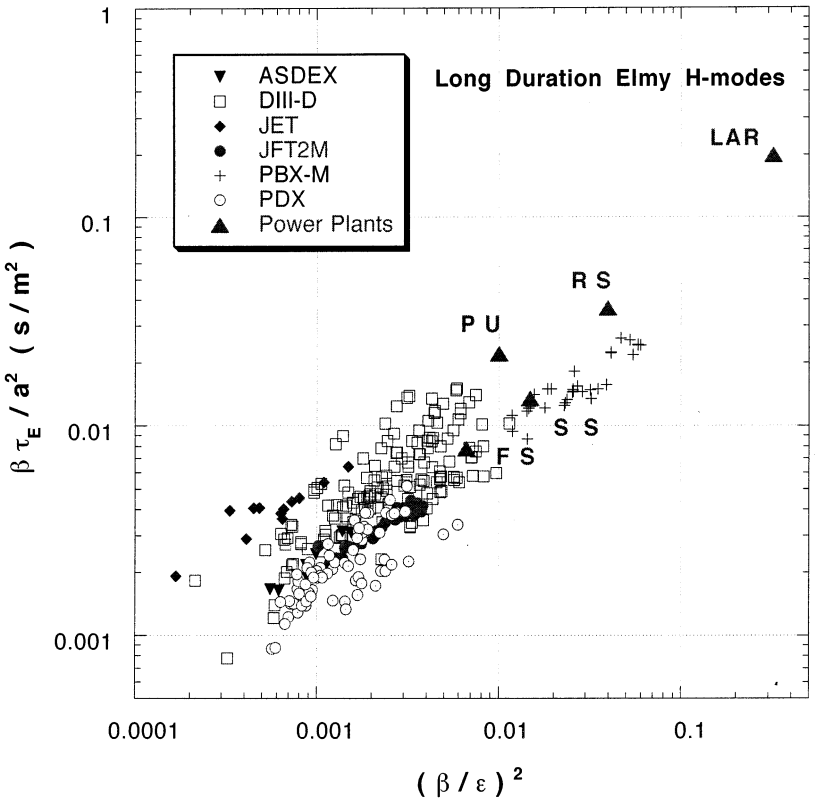

Fig. 4. Energy confinement figures of merit for a number existing tokamaks and the five ARIES fusion power plant designs.

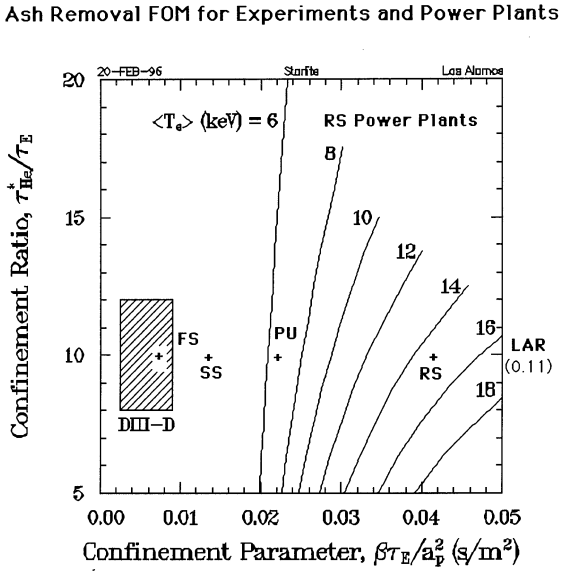

Fig. 5. Ash removal figures of merit for DIII-D ELMy H-mode discharges, for plant candidates, and for ignition in a reversed shear power plant at various temperatures.

- Current drive:
  - Normalized current-drive efficiency: $\gamma_B \equiv \bar{n}_e I_p R/P_{CD}$ versus electron temperature T_e
- Heat exhaust:
  - Normalized heat flux: P_{tr}/R
  - Total radiation fraction: f_{rad}
- Energy confinement:
  - Ignition parameter: $\beta\tau_E/a_p^2$
  - Power density parameter: β/ε
- Helium ash removal:
  - Particle confinement parameter: τ^*_{He}/τ_E
  - Ignition parameter: $\beta\tau_E/a_p^2$
  - Effective charge: Z_{eff}

Values for these figures of merit in the five critical physics areas that were measured in experiments have been plotted along with the design values for the five plant options. Based on the results displayed in these figures, it is clear that the FS and PU power plant options have physics performance parameters that are closest to the existing database. On the other hand, the LAR concept demands the largest physics performance extrapolations.

It is useful to identify physics areas in which to focus present and future research efforts towards prototyping an attractive power plant. We first note that the experimental data that are used in this study are taken entirely from L-mode and H-mode discharges, without the use of any profile tailoring. Thus, a systematic development and collection of database for reverse shear discharges on large high-power devices are in order, including all five aforementioned critical physics areas. Also, all of the experimental data in the ITER data bases came from tokamaks with more conventional aspect ratios, and the inclusion of low aspect ratio data is sorely needed.

It is clear from Fig. 1 that the three designs that rely on a nearby conducting wall to obtain aggressive MHD parameters, (i.e. RS, SS, and LAR) have yet to be experimentally prototyped (with the caveat of the RS parameters being close to the best of the PBX-M high-beta bean shaped discharges). This is a high-leverage area, and we would hope that new theoretical ideas in this area involving driven poloidal rotation [19] and active feedback stabilization [20] can be experimentally tested and eventually prototyped.

From a broader perspective, it is also clear that the database for existing tokamak discharges do not contain any points that simultaneously achieve values of all the physics FOM parameters needed to make an attractive fusion power plant. This highlights the need for continued physics research aimed at concept improvement. There are significant physics issues that needs to be demonstrated in non-DT tokamaks in order to prototype attractive operating regimes for DT tokamaks and eventually for fusion power plants. There is need for demonstration of advanced tokamak operation in each of the areas of MHD, current drive, divertors, and energy confinement. Eventually, these will all have to be demonstrated together.

Finally, we emphasize the need to develop an experimental database in long pulse or steady state discharges with the use of current drive and profile control in fusion relevant regimes. There are many results that have been demonstrated transiently that cannot be sustained for steady state. A realistic assessment of the constraints imposed by steady state or long-pulse requirements will help focus efforts on improvements that are of true practical value.

References

[1] F. Najmabadi, ARIES Team. The ARIES-1 tokamak reactor study. University of California, Los Angeles Report UCLA-PPG-1323 (1991).

[2] F. Najmabadi, ARIES Team. The PULSAR tokamak reactor study. University of California, San Diego Report (to be published).

[3] F. Najmabadi, ARIES Team. The ARIES-II and -IV second stability tokamak reactors. University of California, Los Angeles Report UCLA-PPG-1461 (to be published).

[4] S.C. Jardin, C.E. Kessel, C.G. Bathke, D.A. Ehst, T.K. Mau, F. Najmabadi, T.W. Petrie, The ARIES Team. Physics basis for a reversed shear tokamak power plant. Fusion Eng. Design 38 (1997) 27.

[5] C.E. Kessel, J. Manickam, G. Rewoldt, W.M. Tang, Improved plasma performance in tokamaks with negative magnetic shear, Phys. Rev. Lett. 72 (1994) 1212.

[6] Y.-K.M. Peng, Prospects and status of low-aspect-ratio tokarnaks, Trans. Fusion Technol. 27 (1995) 138.

[7] T.K. Mau, D.A. Ehst, S.C. Jardin, C.E. Kessel, B.J. Lee, Plasma system requirements and performance data base for the starlite/demo fusion power plant. Proc. 16th 1EEEINPS5 Symposium on Fusion Engineering, Champaign, IL (1995) 1194.

[8] C.G. Bathke, The ARIES Team. A preliminary systems assessment of the starlite DEMO candidates. Los Alamos National Laboratory Report LA-UR-95-3489; Proc. 16th 1EEEINPSS Symposium on Fusion Engineering, Champaign, IL (1995) 1139.

[9] C.E. Kessel, Bootstrap current in a tokarnak, Nucl. Fusion 34 (1994) 1221.

[10] F. Levinton, M.C. Zarnstorff, S.H. Batha, et al., Enhanced confinement with reversed magnetic shear in TFTR, Phys. Rev. Lett. 75 (1995) 4417.

[11] E.J. Strait, L.L. Lao, M.E. Mauel, et al., Enhanced confinement and stability in DIII-D discharges with reversed magnetic shear, Phys. Rev. Lett. 75 (1995) 4420.

[12] H.R. Strauss, Dynamics of high β tokarnaks, Phys. Fluids 20 (1977) 1354.

[13] N. Pomphrey, Bootstrap dependence on plasma profile parameters. Princeton Plasma Physics Laboratory Report PPPL-2854 (1992).

[14] P.A. Politzer, T. Casper, C.B. Forest, et al., Evolution of high β_p plasmas with improved stability and confinement, Phys. Plasmas 1545 (1994) 1.

[15] J. Menard, S.C. Jardin, S.M. Kaye, et al., Ideal MHD stability limits of low aspect ratio tokamak plasmas, Nucl. Fusion 37 (1997) 595.

[16] R.L. Miller, Y.R. Lin-Liu, A.D. Turnbull, et al., Stable equilibria for bootstrap-currentdriven low aspect ratio tokamaks, Phys. Plasmas 4 (1997) 1062.

[17] J.J. Ramos, Theory of the tokamak beta limit and implications for second stability, Phys. Fluids B3 (1991) 2247.

[18] M.S. Chance, S.C. Jardin, T. Stix, Ballooning mode stability of bean-shaped cross sections for high-β tokamak plasmas, Phys. Rev. Lett. 51 (1983) 1963.

[19] A. Bondeson, D.J. Ward, Stabilizaton of external modes in tokamaks by resistive walls and plasma rotation, Phys. Rev. Lett. 72 (1994) 2709.

[20] R. Fitzpatrick, Feedback stabilization of the resistive shell mode in a tokamak fusion reactor, Phys. Plasmas 4 (1997) 2519.

[21] D.A. Ehst, C.E. Kessel, R.A. Krakowski, C.G. Batlike, S.C. Jardin, T.K. Mau, F. Najinabadi, Economic comparison of MHD equilibrium options for advanced steady state tokamak power plants. Nucl. Fusion 38 (1998) 13.

[22] N.J. Fisch, Theory of current drive in plasmas, Rev. Mod. Phys. 59 (1987) 175.

[23] D.A. Ehst, K. Evan Jr, Multiple wave radiofrequency current driven tokamak reactors in the first stability regime, Nucl. Fusion 27 (1987) 1267.

[24] D.A. Ehst, C.F.F. Karney, Approximate formula for radiofrequency current drive efficiency with magnetic trapping, Nucl. Fusion 31 (1991) 1933.

[25] D.A. Ehst, K. Evans Jr, D.W. Ignat, Tokamak MHD equilibrium generation by narrow-spectrum fast-wave current drive, Nucl. Fusion 26 (1986) 461.

[26] K. Lackner, Figures of merit for divertor similarity, Comm. Plasma Phys. Contr. Fusion 15 (1994) 359.

[27] P.J. Catto, S. Krasheninnikov, J.W. Conner. Scaling laws for two-dimensional divertor modeling. MIT report PFC/JA-95-10 (1995).

[28] P.J. Catto, A short mean-free path, coupled neutral-ion transport description of a tokamak edge plasma, Phys. Plasmas 1 (1994) 1936.

[29] P. Yushmanov, T. Takizuka, K.S. Riedel, et al., Scalings for tokamak energy confinement, Nucl. Fusion 30 (1990) 1999.

[30] F. Perkins, P. Barabaschi, G. Bosia, et al.@, ITER physics basis, in: Plasma Phys. and Controlled Nucl. Fusion Res., (Proc. 15th Int. Conf., Seville, 1994) IAEA-CN60/E-1-1-3.

[31] J. Sheffield, Physics requirements for an attractive magnetic fusion reactor, Nucl. Fusion 25 (1985) 1733.

[32] R.J. Goldston, S.H. Batha, R.H. Bulmer, et al., Advanced tokamak physics-status and prospects, Plasma Phys. Control. Fusion 36 (1994) B213.

[33] S.M. Kaye, The ITER Joint Central Team and Home Teams. Projection of ITER performance using the multimachine L- and H-mode databases, in: Plasma Phys. and Controlled Nucl. Fusion Res., (Proc. 15th Int. Conf., Seville, 1994) IAEAXN60/E-P-3.

[34] A. Sykes, G.W. Crawford, G. Cunningham, et al., The START spherical tokamak, to appear in: Proc. 16th 1EEEINP5S Symp. on Fusion Engineering, Champaign, IL (1995).

[35] D. Reiter, G. Wolf, H. Kever, Burn condition, helium particle confinement and exhaust efficiency, Nucl. Fusion 30 (1990) 2141.

[36] R. Behrisch, V. Prozesky, Particle and power exhaust for a fusion plasma, Nucl. Fusion 30 (1990) 2166.

[37] R.J. Taylor, B.D. Fried, G.J. Morales, Burn threshold for fusion plasmas with helium accumulation, Comm. Plasma Phys. 13 (1990) 227.
[38] A. Bondeson, M. Benda, M. Persson, Magnetohydrodynamic beta limits for tokamaks with negative central shear, Nucl. Fusion 37 (1997) 1419.
[39] J.S. deGrassie, C.C. Petty, R.I. Pinsker, et al. Fast wave current drive on DIII-D, Proc. 11th Top. Conf. on Radio Frequency Power in Plasmas, Palm Springs, CA (1995) 173. Data point at $T_{e0} = 6.3$ keV is unpublished and provided by C.C. Petty.
[40] X. Litaudon for Equipe Tore Supra, RF Heating and Current Drive in Tore Supra, in: 11th Top. Conf. on Radio Frequency Power in Plasmas, Palm Springs, CA (1995). Data point from R. Goldston.
[41] J.H. Rogers, PPPL, private communication (1995).
[42] C. Gormezano for the JET Team. Non-inductive current drive in JET, in: Plasma Phys. and Controlled Nucl. Fusion Research, Proc. 14th Int. Conf., Wiirzburg, Germany (1992) 587.
[43] T. Imai, H. Kimura, Y. Kusama, et al., Lower hybrid current drive and higher harmonic ICRF heating experiments on JT-60, in: Plasma Phys. and Controlled Nucl. Fusion Research (Proc. 13th IAEA Conf., Washington, DC) Vol. 1 (1990) 645.
[44] Technical Meeting and Workshop on ITER Divertor Physics Design, ITER Joint Work Site Garching (1994).
[45] U. Samm, G. Bertchinger, P. Bogen, et al., Radiative edges under control by impurity fluxes, Plasma Phys. Control. Fusion 35 (1993) B167.
[46] J. Neuhauser and the ASDEX-Upgrade Teams, The compatibility of high confinement times and complete divertor detachment in ASDEX-Upgrade, Proc. 22nd EPS Conf. on Controlled Fusion and Plasma Physics, Bournemouth, UK (1995) 139.
[47] A.W. Leonard, S.L. Allen, M.E. Fenstermacher, et al. Radiation distributions in detached divertor operation on DIII-D, General Atomics report GA-A22068; also in Proc. 22nd EPS Conf. on Controlled Fusion and Plasma Phys., Bournemouth, UK (1995).
[48] D.L. Hillis, K.H. Finken, J.T. Hogan, et al., Helium exhaust and transport studies with the ALT-11 pump limiter in the TEXTOR tokarnak, Phys. Rev. Lett. 65 (1990) 2382.
[49] D.L. Hillis, J.T. Hogan, K.H. Finken, et al., Helium transport in enhanced confinement regimes on the TEXTOR and DIII-D tokarnaks, J. Nucl. Mat. 196-198 (1992) 35.
[50] M.R. Wade, D.L. Hillis, J.T. Hogan, et al., Helium exhaust studies in H-mode discharges in the DIII-D tokamak using an argon-frosted divertor cryopump, Phys. Rev. Lett. 74 (1995) 2702.
[51] M.R. Wade, D.L. Hillis, J.T. Hogan, et al., Helium transport and exhaust studies in enhanced confinement regimes in DIII-D, Phys. Plasmas 2 (1995) 2357.